

## Topological magnon modes in a chain of magnetic spheres


Faezeh Pirmoradian,<sup>1</sup> Babak Zare Rameshti,<sup>2,3</sup> MirFaez Miri,<sup>4,\*</sup> and Shahpoor Saeidian<sup>1</sup>

<sup>1</sup>*Department of Physics, Institute for Advanced Studies in Basic Sciences (IASBS), Zanjan 45137-66731, Iran*

<sup>2</sup>*Department of Physics, Iran University of Science and Technology, Narmak, Tehran 16844, Iran*

<sup>3</sup>*School of Physics, Institute for Research in Fundamental Sciences (IPM), 19395-5531, Tehran, Iran*

<sup>4</sup>*Department of Physics, University of Tehran, P. O. Box 14395-547, Tehran, Iran*

 (Received 29 August 2018; revised manuscript received 24 October 2018; published 6 December 2018)

We study the collective magnonic modes of a one-dimensional bipartite chain of magnetic spheres coupled by dipolar interactions. The magnonic modes of the *infinite* chain, due to the dipolar interaction, give rise to a gapped magnonic dispersion. The external magnetic fields can be invoked to quantize the Zak phase of the magnonic bands, which is used as an invariant to identify two topologically distinct phases of the system. In the case of a *finite* chain, the magnetic fields determine whether topologically protected localized states or Tamm-like states form at the ends of the chain. We provide an analytical expression along with numerical results which reveal parameters resulting in topologically protected end states. This bosonic system is almost similar to the Su–Schrieffer–Heeger system and is promising as a dynamically reconfigurable material for future use in magnonics.

DOI: [10.1103/PhysRevB.98.224409](https://doi.org/10.1103/PhysRevB.98.224409)

### I. INTRODUCTION

Spin waves (SWs) are the collective propagation of coupled precessing spins in a polarized spin system and magnons, the quanta of collective motion, can be exploited as information and energy carriers [1–5]. Spectra of SW excitations in artificial structures with periodic variations in their magnetic properties [6,7] are significantly different compared with uniform media and show distinctive features such as band gaps, the frequency intervals in which SWs are not allowed to propagate [8–21]. Such artificial magnetic materials, dubbed “magnonic crystals” (MCs) and which can be regarded as the magnetic counterpart of photonic [22,23] or phononic [24,25] crystals that guide SWs rather than electromagnetic or elastic waves, would coherently transport magnetic energy and information. The possibility of using SWs as an alternative means for information processing over a broad frequency range stimulates the so-called magnonics aimed at manipulating the generation and propagation of SWs. Although MCs are used for dipolar or exchange-coupled constituent materials [26], the coherent coupling of magnonic atoms via an intermediary will also form MCs [27,28], opening a new possibility to design material properties for SWs.

MCs, the building blocks of magnonics, owing to special characteristics of SWs spectra, are used in tunable phase shifters [29], magnetic sensors [30], and transistors [31]. Furthermore, MCs offer a unique platform which has several advantages over photonic or phononic devices, because they can be easily modified by applying a magnetic field. Intriguingly, the band gaps can be manipulated not only by changing crystal parameters and using various materials but also by tuning the direction and strength of the applied magnetic field.

These unprecedented features pave the way for reconfigurable magnonic devices which show reprogrammable tailored band structures [6].

On the other hand, the key features of topological phases in condensed matter have transferred to the realm of photonics, phononics, and magnonics. The potentially nontrivial topological properties of collective excitations in photonic [32–34] and phononic [35–38] metamaterials were uncovered. Recently, known topological effects in fermionic systems found their analogues in bosonic systems, such as in the experimental realizations of one-way topologically protected edge states. By invoking time-reversal symmetry breaking, a photonic analog of a quantum Hall phase with chiral edge modes was proposed [39–41] and the existence of such robust edge modes were experimentally observed shortly afterward [42]. The protected unidirectional propagation of elastic edge waves were also reported in phononic crystals [43]. Moreover, spin and valley Hall effects which demand breaking of spatial symmetry were demonstrated by using photonic [44–47] and phononic [48,49] topological insulators. Other artificial systems such as photonic lattices [50,51], and dielectric resonators [52,53], were also shown to present interesting nontrivial topological features. Many studies are devoted to topologically protected edge states of interacting spins on a lattice [54–57]. However, topological phases of artificial magnetic structures are less explored.

The Su–Schrieffer–Heeger (SSH) model proposed to describe the transport properties of one-dimensional polyacetylene [58] has raised attention to the topological phases of matter. The SSH model exhibits rich physical phenomena, such as fractional charge [59], nontrivial end states [60,61], and topological soliton states [62]. The transition between trivial and topological phases of the SSH model is associated with the number of midgap edge states as the topological invariant. The SSH model is realized with a phononic crystal

\*mirfaez\_miri@ut.ac.ir

waveguide [63], and cold atoms in one-dimensional optical lattices [64]. It is also simulated in a photonic crystal excited with a laser light [65] and in a transmission line excited with a microwave source [66].

To realize a bosonic system almost similar to the SSH system, we introduce a magnonic crystal rather than a photonic or a phononic crystal. In this paper, we address the collective magnonic modes of a linear bipartite chain of dipolarly coupled magnetic spheres which are subjected to external magnetic fields. The spin-wave properties of our system are to some extent analogous to the electronic properties of the SSH system. Despite the absence of chiral symmetry, the magnonic crystal exhibits rich physics. Due to the dipolar interactions in an *infinite* chain of magnetic spheres, a two-band magnonic band structure arises which has a small gap at the edge of the first Brillouin zone. Upon tuning the parameters of the system, especially applied magnetic fields, the Zak phase of the magnonic bands becomes quantized and reveals two topologically distinct phases of the system. The phase transition is accompanied by closing and re-opening the energy gap. In the case of a *finite* chain, the external magnetic fields determine whether topologically protected localized states or Tamm-like states form at the ends of the chain. The chain of magnetic spheres is of fundamental interest due to its inherent topologically nontrivial phases and its tunability by applied magnetic fields, which makes it promising as a dynamically reconfigurable material for future use in magnonics.

This paper is organized as follows: In Sec. II, we introduce our model for collective excitations in a chain of magnetic spheres. The topological properties of the magnonic band structure of the chain, and the appearance of different kinds of end states, are discussed in Secs. III and IV, respectively. In Sec. V we investigate the formation of localized edge state at the interface between two topologically distinct chains. Our analytical and numerical results regarding the appearance of two types of end modes are discussed in Sec. VI. In Sec. VII, we conclude and summarize our findings.

## II. MODEL

We consider a one-dimensional bipartite lattice composed of  $N$  unit cells (see Fig. 1). The intra- and intercell distances between adjacent sites are  $d_1$  and  $d_2$ , respectively. The distance between sites of the same type is  $d = d_1 + d_2$ . The  $n$ th unit cell contains two magnetic spheres possessing macrospins  $\hat{\mathbf{S}}_n = (\hat{S}_n^x, \hat{S}_n^y, \hat{S}_n^z)$  and  $\hat{\mathbf{S}}'_n = (\hat{S}'_n{}^x, \hat{S}'_n{}^y, \hat{S}'_n{}^z)$ . We assume that  $\hat{S}_n^2 = S_1(S_1 + 1)\hbar^2$  and  $\hat{S}'_n{}^2 = S_2(S_2 + 1)\hbar^2$ , which are the magnitudes of spins at equivalent sites, are the same. A constant magnetic induction  $\mathbf{B}_1 = B_1\mathbf{e}_z$  ( $\mathbf{B}_2 = B_2\mathbf{e}_z$ ) saturates the equilibrium magnetization of an  $S_1$ -type ( $S_2$ -type) sphere. The outermost left and right sites of the chain experience additional magnetic inductions  $\delta\mathbf{B}_L = \delta B_L\mathbf{e}_z$  and  $\delta\mathbf{B}_R = \delta B_R\mathbf{e}_z$ , respectively. We explore the effect of the additional magnetic inductions in detail.

The dipole moments of magnetic spheres in the chain are coupled through the dipole-dipole interaction. The model Hamiltonian that describes the collective excitation in the

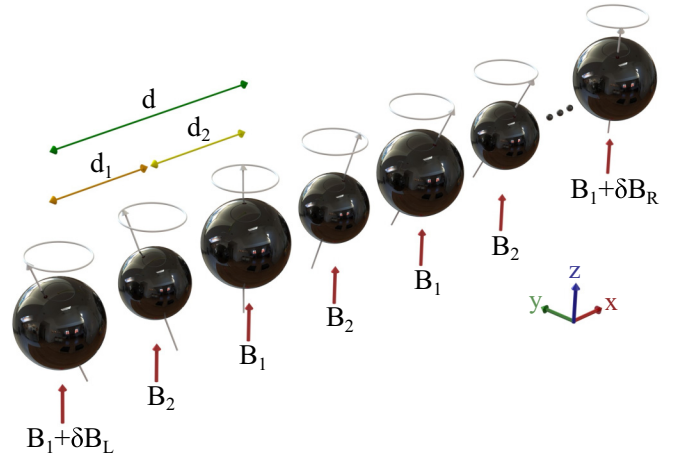


FIG. 1. A linear bipartite chain of magnetic spheres, with a unit cell consisting of two spheres of macrospins,  $S_1$  and  $S_2$ . The intra- and intercell separation between neighboring sites are  $d_1$  and  $d_2$ , respectively. A constant magnetic induction  $\mathbf{B}_1$  ( $\mathbf{B}_2$ ) saturates the equilibrium magnetization of a  $S_1$ -type ( $S_2$ -type) sphere. The outermost left and right sites experience additional magnetic inductions  $\delta\mathbf{B}_L$  and  $\delta\mathbf{B}_R$ , respectively.

bipartite chain of magnetic spheres reads

$$\begin{aligned}
 H = & \frac{\mu_0\mu^2}{4\pi d_1^3} \sum_{n=1}^N [\hat{\mathbf{S}}_n \cdot \hat{\mathbf{S}}'_n - 3(\hat{\mathbf{S}}_n \cdot \mathbf{e}_x)(\hat{\mathbf{S}}'_n \cdot \mathbf{e}_x)] \\
 & + \frac{\mu_0\mu^2}{4\pi d_2^3} \sum_{n=1}^{N-1} [\hat{\mathbf{S}}_{n+1} \cdot \hat{\mathbf{S}}'_n - 3(\hat{\mathbf{S}}_{n+1} \cdot \mathbf{e}_x)(\hat{\mathbf{S}}'_n \cdot \mathbf{e}_x)] \\
 & - \mu B_1 \sum_{n=1}^N \hat{S}_n^z - \mu B_2 \sum_{n=1}^N \hat{S}'_n{}^z, \quad (1)
 \end{aligned}$$

where  $\mu_0$  is the vacuum permeability, and  $\mu = g\mu_B/\hbar$  in which  $g$  and  $\mu_B$  are the  $g$  factor and the Bohr magneton, respectively. We have neglected the dipole-dipole interactions beyond the nearest neighbors, since these interactions do not change the main picture.

In the ground state of the system, all macrospins are aligned parallel to the applied magnetic field. Although macrospins are large, the quantum nature of low-temperature macrospin-fluctuations must be respected. Being interested in the low-energy collective excitations of the system, we use the Holstein–Primakoff transformation to rewrite the Hamiltonian in terms of the spin-deviation operators. We express the spin operator  $\hat{\mathbf{S}}$  ( $\hat{\mathbf{S}}'$ ) in terms of the bosonic operator  $\hat{\mathbf{a}}$  ( $\hat{\mathbf{b}}$ ) as

$$\begin{aligned}
 \hat{S}^+ &= \hbar\sqrt{2S_1}\hat{\mathbf{a}}, & \hat{S}'^+ &= \hbar\sqrt{2S_2}\hat{\mathbf{b}}, \\
 \hat{S}^- &= \hbar\sqrt{2S_1}\hat{\mathbf{a}}^\dagger, & \hat{S}'^- &= \hbar\sqrt{2S_2}\hat{\mathbf{b}}^\dagger, \\
 \hat{S}^z &= \hbar(S_1 - \hat{\mathbf{a}}^\dagger\hat{\mathbf{a}}), & \hat{S}'^z &= \hbar(S_2 - \hat{\mathbf{b}}^\dagger\hat{\mathbf{b}}). \quad (2)
 \end{aligned}$$

Note that the commutation relations of the spin operators  $\hat{S}^\pm = \hat{S}^x \pm i\hat{S}^y$  and  $\hat{S}'^\pm = \hat{S}'^x \pm i\hat{S}'^y$  imply that  $[\hat{\mathbf{a}}, \hat{\mathbf{a}}^\dagger] = 1$  and  $[\hat{\mathbf{b}}, \hat{\mathbf{b}}^\dagger] = 1$ . The Hamiltonian (1) can be written in terms

of the bosonic operators as

$$\begin{aligned}
 H = & -\sqrt{S_1 S_2} \frac{\mu_0 \hbar^2 \mu^2}{8\pi d_1^3} \sum_{n=1}^N (\hat{\mathbf{a}}_n \hat{\mathbf{b}}_n^\dagger + 3\hat{\mathbf{a}}_n \hat{\mathbf{b}}_n + \text{H.c.}) \\
 & -\sqrt{S_1 S_2} \frac{\mu_0 \hbar^2 \mu^2}{8\pi d_2^3} \sum_{n=1}^{N-1} (\hat{\mathbf{a}}_{n+1} \hat{\mathbf{b}}_n^\dagger + 3\hat{\mathbf{a}}_{n+1} \hat{\mathbf{b}}_n + \text{H.c.}) \\
 & -\frac{\mu_0 \hbar^2 \mu^2}{4\pi d_2^3} \sum_{n=1}^{N-1} (S_2 \hat{\mathbf{a}}_{n+1}^\dagger \hat{\mathbf{a}}_{n+1} + S_1 \hat{\mathbf{b}}_n^\dagger \hat{\mathbf{b}}_n) \\
 & + \hbar \mu \left[ B_1 - \frac{\mu_0 \hbar \mu}{4\pi d_1^3} S_2 \right] \sum_{n=1}^N \hat{\mathbf{a}}_n^\dagger \hat{\mathbf{a}}_n \\
 & + \hbar \mu \left[ B_2 - \frac{\mu_0 \hbar \mu}{4\pi d_1^3} S_1 \right] \sum_{n=1}^N \hat{\mathbf{b}}_n^\dagger \hat{\mathbf{b}}_n + E_0, \quad (3)
 \end{aligned}$$

where all terms containing the product of four operators have been neglected. Hereafter  $E_0 = -N\hbar\mu(B_1 S_1 + B_2 S_2) + \mu_0 \hbar^2 \mu^2 S_1 S_2 [N/d_1^3 + (N-1)/d_2^3]/(4\pi)$  serves as the zero of the energy.

It has been theoretically anticipated [67] and experimentally demonstrated [68–70] that macrospins—strongly exchange-coupled spins in a ferromagnetic or ferrimagnetic material—are promising: Using the high spin density of ferromagnets or ferrimagnets and a microwave cavity, even the ultrastrong-coupling regime of the light-matter interaction is reachable [70]. Inspired by the experiment of Tabuchi *et al.* [69], we assume that spheres are made of the ferrimagnet yttrium iron garnet (YIG) with a spin density  $\sim 2 \times 10^{28} \mu_B \text{ m}^{-3}$ . For spheres of diameter  $\sim 1 \mu\text{m}$ , we find  $S_{1,2} \sim 10^{10}$ . Typically  $d_{1,2} \sim 3\text{--}10 \mu\text{m}$  and  $B_{1,2} \sim 0.1\text{--}1 \text{ T}$ .

### III. COLLECTIVE EXCITATIONS IN AN INFINITE CHAIN OF MAGNETIC SPHERES

We first concentrate on an *infinite* chain of magnetic spheres to identify the possible topologically distinct phases of the bulk. This is of great use when we consider a finite chain or an interface between two topologically distinct chains, since there is a link between the bulk topological invariant and the presence of topologically protected end states. Indeed, the bulk-boundary correspondence is a recurrent theme in the theory of topological insulators.

The physical properties of an infinite chain do not depend on its ends, thus we adopt periodic boundary conditions and rewrite the Hamiltonian (3) in the momentum space. Due to the translational invariance of the system, the Hamiltonian in the basis  $\Phi_k^\dagger = (\hat{\mathbf{a}}_k^\dagger, \hat{\mathbf{b}}_k^\dagger, \hat{\mathbf{a}}_{-k}, \hat{\mathbf{b}}_{-k})$  can be written as  $H = \sum_k \Phi_k^\dagger \mathcal{H}(k) \Phi_k$ , where  $\mathcal{H}(k)$  is given by

$$\mathcal{H}(k) = \tau_0 \otimes M_0 + (\tau_0 + 3\tau_x) \otimes M_1(k), \quad (4)$$

$$M_0 = \begin{bmatrix} \zeta_1 & 0 \\ 0 & \zeta_2 \end{bmatrix}, \quad M_1(k) = \begin{bmatrix} 0 & \eta_k \\ \eta_k^* & 0 \end{bmatrix}, \quad (5)$$

where  $\tau_i$  refers to Pauli matrices,  $\tau_0$  is the identity matrix, and  $k$  is the lattice momentum. Here we have defined  $\zeta_1 = 2(w_1 + w_2)\sqrt{S_2/S_1} + \hbar\mu B_1$ ,  $\zeta_2 = 2(w_1 +$

$w_2)\sqrt{S_1/S_2} + \hbar\mu B_2$ , and  $\eta_k = w_1 + w_2 e^{-ikd}$  in terms of  $w_1 = -\mu_0 \hbar^2 \mu^2 \sqrt{S_1 S_2}/(8\pi d_1^3)$  and  $w_2 = w_1 d_1^3/d_2^3$ . It can easily be verified that, when  $\zeta_1 = \zeta_2$ , the Hamiltonian has an inversion symmetry  $\mathcal{I}\mathcal{H}(k)\mathcal{I}^{-1} = \mathcal{H}(-k)$  with respect to the unitary operators  $\mathcal{I} = \tau_0 \otimes \tau_x$  and  $\mathcal{I} = \tau_x \otimes \tau_x$ . Moreover,  $\mathcal{C}\mathcal{H}(k)\mathcal{C}^{-1} = \mathcal{H}(-k)$ , where  $\mathcal{C} = \tau_x \otimes \tau_0 \mathcal{K}_c$ , with  $\mathcal{K}_c$  being the complex-conjugate operator, which implies that, if  $|k\rangle$  is an eigenvector of  $\mathcal{H}(k)$  with energy  $\varepsilon(k)$ , then another solution is given by  $\mathcal{C}|k\rangle$  with energy  $\varepsilon(-k)$ . The Hamiltonian has no chiral symmetry.

The Hamiltonian  $H$  can be diagonalized by a Bogoliubov transformation given by

$$\begin{aligned}
 \hat{\mathbf{c}}_{1k} &= o_{1k} \hat{\mathbf{a}}_k + p_{1k} \hat{\mathbf{b}}_k + q_{1k} \hat{\mathbf{a}}_{-k}^\dagger + v_{1k} \hat{\mathbf{b}}_{-k}^\dagger, \\
 \hat{\mathbf{c}}_{2k} &= o_{2k} \hat{\mathbf{a}}_k + p_{2k} \hat{\mathbf{b}}_k + q_{2k} \hat{\mathbf{a}}_{-k}^\dagger + v_{2k} \hat{\mathbf{b}}_{-k}^\dagger. \quad (6)
 \end{aligned}$$

Rewritten in terms of the introduced quasiparticles the Hamiltonian (3) takes the form

$$H = \sum_k (E_{1k} \hat{\mathbf{c}}_{1k}^\dagger \hat{\mathbf{c}}_{1k} + E_{2k} \hat{\mathbf{c}}_{2k}^\dagger \hat{\mathbf{c}}_{2k}). \quad (7)$$

The Heisenberg equations of motion  $[\hat{\mathbf{c}}_{1k}, H] = E_{1k} \hat{\mathbf{c}}_{1k}$  and  $[\hat{\mathbf{c}}_{2k}, H] = E_{2k} \hat{\mathbf{c}}_{2k}$  then yield

$$\begin{bmatrix} \zeta_1 & \eta_k^* & 0 & -3\eta_k^* \\ \eta_k & \zeta_2 & -3\eta_k & 0 \\ 0 & 3\eta_k^* & -\zeta_1 & -\eta_k^* \\ 3\eta_k & 0 & -\eta_k & -\zeta_2 \end{bmatrix} \begin{bmatrix} o_{1,2k} \\ p_{1,2k} \\ q_{1,2k} \\ v_{1,2k} \end{bmatrix} = E_{1,2k} \begin{bmatrix} o_{1,2k} \\ p_{1,2k} \\ q_{1,2k} \\ v_{1,2k} \end{bmatrix}. \quad (8)$$

The quasiparticles in Eq. (7) thus correspond to the excitations of the chain, and their energies are

$$\begin{aligned}
 E_{1,2k}^2 = & -8|\eta_k|^2 + \frac{1}{2}(\zeta_1^2 + \zeta_2^2) \pm [|\eta_k|^2(\zeta_1 + \zeta_2)^2 \\
 & + (\zeta_1 - \zeta_2)^2(\frac{1}{4}(\zeta_1 + \zeta_2)^2 - 9|\eta_k|^2)]^{\frac{1}{2}}. \quad (9)
 \end{aligned}$$

In the vicinity of the edges of the first Brillouin zone, we write  $kd = \pm\pi + k_e d$  where  $|k_e d| \ll 1$ . It follows that the energy spectrum  $E_{1,2k_e}$  resembles the massive relativistic energy spectrum  $E = \pm(m^2 c^4 + p^2 c^2)^{1/2}$ . In particular, for  $\zeta_1 = \zeta_2 \gg |w_{1,2}|$ , we find that  $E_{1,2k_e} = \zeta_1 \pm [(w_1 - w_2)^2 + w_1 w_2 k_e^2 d^2]^{1/2}$ , where two magnonic bands are symmetric with respect to the energy  $\zeta_1$ .

The spectrum has an overall nonzero gap, which however can be made zero at  $kd = \pm\pi$ , for  $|\eta_k|^2(\zeta_1 + \zeta_2)^2 + (\zeta_1 - \zeta_2)^2[\frac{1}{4}(\zeta_1 + \zeta_2)^2 - 9|\eta_k|^2] = 0$ . This implies that the gap closes if simultaneously  $w_1 = w_2$  and  $\zeta_1 = \zeta_2$ , for which  $E_{1k} = E_{2k} = \zeta_1$ . Figure 2(a) shows the bulk excitation spectrum of the chain  $E_{1,2k}$  as a function of  $kd$  for different values of  $w_1/w_2$  and for the special case  $\zeta_1 = \zeta_2$ . The two limiting cases of  $w_1 \neq 0, w_2 = 0$  and  $w_1 = 0, w_2 \neq 0$ , with gaped dispersion in which intracoupling and intercoupling are dominant, respectively, correspond to different dimerized regimes and hence indicate that a transition must occur somewhere in between these two limits. For  $w_1/w_2 > 1$  the system is in a topologically trivial phase, while for  $w_1/w_2 < 1$  the chain is in a topological phase and the transition is characterized by closing and re-opening the gap at  $w_1/w_2 = 1$ .

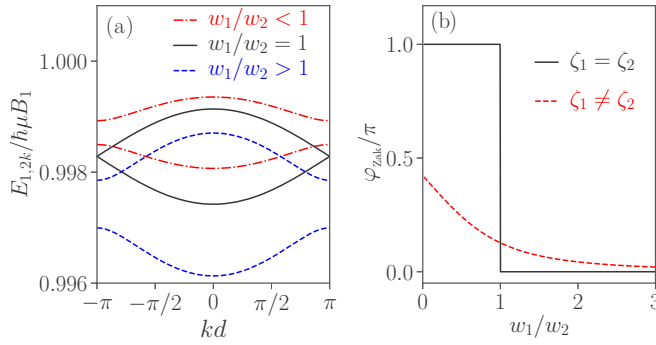


FIG. 2. (a) The energy spectrum of the Bogoliubov quasiparticle excitations of the chain  $E_{1,2k}$  versus  $kd$  for  $\zeta_1 = \zeta_2$  and  $w_1/w_2 \in \{0.5, 1, 2\}$ . (b) The Zak phase  $\varphi_{Zak}$  versus  $w_1/w_2$  for both  $\zeta_1 = \zeta_2$  and  $\zeta_1 \neq \zeta_2$ . Here  $S_2/S_1 \in \{1, 2\}$  are exemplified. In all plots  $B_1 = B_2 = 0.1$  T,  $d_2 = 6 \mu\text{m}$  and  $S_1 = 10^{10}$ .

There is a close similarity between the chain of magnetic spheres and the SSH system hence our system supports topological edge states inherited from the SSH model. To demonstrate this, we calculate the Zak phase [71] defined by

$$\varphi_{Zak} = -i \int_{1^{\text{st}} \text{ BZ}} \langle \Psi_{1,2k} | \partial_k | \Psi_{1,2k} \rangle_B dk, \quad (10)$$

where  $|\Psi_{1,2k}\rangle = [\rho_{1,2k}, p_{1,2k}, q_{1,2k}, v_{1,2k}]^T$  is the eigenvector of  $H$  and the integral is taken over the first Brillouin zone. It should be noted that, for bosonic eigenstates, we have  $\langle \Psi_1 | \Psi_2 \rangle_B = \langle \Psi_1 | \tau_z \otimes \tau_0 \Psi_2 \rangle$  [72]. Figure 2(b) shows the Zak phase as a function of  $w_1/w_2$ . For  $\zeta_1 = \zeta_2$  the Zak phase is quantized, revealing two topologically distinct phases, while it is a continuous function of  $w_1/w_2$  for  $\zeta_1 \neq \zeta_2$ .

#### IV. EDGE STATES IN A FINITE CHAIN OF MAGNETIC SPHERES

The quantization of the Zak phase of the magnonic bands infers the end modes which form in a *finite* chain of magnetic spheres. To gain deeper insight into the end modes, in the following consistent analytical and numerical treatments of end states will be presented.

##### A. Analytical treatment

We have found that a nontrivial phase may exist if  $\zeta_1 = \zeta_2$  which can be fulfilled assuming that  $S_1 = S_2$  and  $B_1 = B_2$ . It follows that

$$-\frac{\mu_0 \hbar^2 \mu^2}{4\pi d_1^3} S_2 + \hbar \mu B_1 = -\frac{\mu_0 \hbar^2 \mu^2}{4\pi d_1^3} S_1 + \hbar \mu B_2 \equiv \tau. \quad (11)$$

However, due to the presence of the additional magnetic inductions  $\delta B_L \equiv \delta_L/(\hbar\mu)$  and  $\delta B_R \equiv \delta_R/(\hbar\mu)$ , the ‘‘onsite energies’’ at the outermost left and right sites of the chain are  $\tau + \delta_L$  and  $\tau + \delta_R$ , respectively. We will show that the difference between the outermost and the bulk onsite energies strikingly affects the nature of the edge states.

We rely on a sort of ‘‘rotating wave approximation’’ (RWA) to neglect  $\hat{\mathbf{a}}_n^\dagger \hat{\mathbf{b}}_n^\dagger$  and similar terms in the Hamiltonian (3). Note that, according to the sub-Hamiltonian  $\zeta_1 \sum_{n=1}^N \hat{\mathbf{a}}_n^\dagger \hat{\mathbf{a}}_n +$

$\zeta_2 \sum_{n=1}^N \hat{\mathbf{b}}_n^\dagger \hat{\mathbf{b}}_n$ , the terms like  $\hat{\mathbf{a}}_n^\dagger \hat{\mathbf{b}}_n^\dagger$  oscillate at frequency  $(\zeta_1 + \zeta_2)/\hbar$ . The neglect of quickly rotating terms of the Hamiltonian (3) is valid when this frequency  $(\zeta_1 + \zeta_2)/\hbar$  is much larger than the hopping frequencies  $|w_1|/\hbar$  and  $|w_2|/\hbar$ . The approximate Hamiltonian can be written as  $H = \Phi^\dagger \mathfrak{h} \Phi$  where  $\Phi^\dagger = [\hat{\mathbf{a}}_1^\dagger, \hat{\mathbf{b}}_1^\dagger, \dots, \hat{\mathbf{a}}_N^\dagger, \hat{\mathbf{b}}_N^\dagger]$  and  $\mathfrak{h}$  is given by

$$\mathfrak{h} = \begin{bmatrix} \tau + \delta_L & w_1 & 0 & 0 & \cdots & 0 & 0 & 0 \\ w_1 & \zeta_1 & w_2 & 0 & \cdots & 0 & 0 & 0 \\ 0 & w_2 & \zeta_1 & w_1 & \cdots & 0 & 0 & 0 \\ \vdots & \vdots & \ddots & \ddots & \ddots & \vdots & \vdots & \vdots \\ 0 & 0 & 0 & 0 & \cdots & w_2 & \zeta_1 & w_1 \\ 0 & 0 & 0 & 0 & \cdots & 0 & w_1 & \tau + \delta_R \end{bmatrix}. \quad (12)$$

We look for eigenstate  $|\psi\rangle = [\mathbb{A}_1, \mathbb{B}_1, \dots, \mathbb{A}_N, \mathbb{B}_N]^T$  of  $\mathfrak{h}$ . The equation  $\mathfrak{h}|\psi\rangle = E|\psi\rangle$  yields

$$(\tau + \delta_L)\mathbb{A}_1 + w_1\mathbb{B}_1 = E\mathbb{A}_1, \quad (13)$$

$$w_1\mathbb{A}_N + (\tau + \delta_R)\mathbb{B}_N = E\mathbb{B}_N, \quad (14)$$

$$w_1\mathbb{A}_n + \zeta_1\mathbb{B}_n + w_2\mathbb{A}_{n+1} = E\mathbb{B}_n, \quad (15)$$

$$w_2\mathbb{B}_{n-1} + \zeta_1\mathbb{A}_n + w_1\mathbb{B}_n = E\mathbb{A}_n, \quad (16)$$

where  $1 < n < N$ . It is convenient to introduce  $\mathbb{A}_{N+1}$  and  $\mathbb{B}_0$  and adopt the recurrence equations (15) and (16) for  $1 \leq n \leq N$ . Then, Eqs. (13) and (14) can be replaced with

$$(\tau + \delta_L - \zeta_1)\mathbb{A}_1 = w_2\mathbb{B}_0, \quad (17)$$

$$w_2\mathbb{A}_{N+1} = (\tau + \delta_R - \zeta_1)\mathbb{B}_N. \quad (18)$$

Note that the energy  $E$  does not appear explicitly in the above boundary conditions.

We assume that the end states are exponentially decaying with distance into the bulk from the boundaries, and consider the ansatz  $\mathbb{A}_l = \mathbb{A}_0 z_{\text{es}}^l$  and  $\mathbb{B}_l = \mathbb{B}_0 z_{\text{es}}^l$ , where  $0 \leq l \leq N+1$ , and  $\mathbb{A}_0, \mathbb{B}_0$ , and  $z_{\text{es}}$  are complex numbers. Indeed,  $z_{\text{es}}$ , or the localization length

$$d_{\text{es}} = \frac{d}{|\ln |z_{\text{es}}||}, \quad (19)$$

characterize the decay of the edge state. For large values of  $N$ , the eigenstate  $|\psi_L\rangle$  localized at the left end and the eigenstate  $|\psi_R\rangle$  localized at the right end can be studied separately. First we focus on the left localized eigenmode  $|\psi_L\rangle$ . By substituting the above ansatz in Eqs. (15)–(17), we find

$$0 = \frac{w_1}{w_2} (\tau + \delta_L - \zeta_1)^2 z_{\text{es}}^2 + [(\tau + \delta_L - \zeta_1)^2 - w_2^2] z_{\text{es}} - w_1 w_2, \quad (20)$$

$$E = \frac{w_1}{w_2} z_{\text{es}} (\tau + \delta_L - \zeta_1) + \tau + \delta_L. \quad (21)$$

Note that here only the solution with  $|z_{es}| < 1$  is admissible. The normalized eigenstate is

$$|\psi_L\rangle = \frac{1}{|z_{es}|} \sqrt{\frac{1}{1 + |z_{es}|^2 \left(\frac{\zeta_1 - \tau - \delta_L}{w_2}\right)^2} \frac{1 - |z_{es}|^2}{1 - |z_{es}|^{2N}}} \times \left[ z_{es}, \frac{\tau + \delta_L - \zeta_1}{w_2} z_{es}^2, \dots, z_{es}^N, \frac{\tau + \delta_L - \zeta_1}{w_2} z_{es}^{N+1} \right]^T. \quad (22)$$

A similar analysis for the right localized eigenmode ends up with

$$|\psi_R\rangle = \frac{1}{|z_{es}|^N} \sqrt{\frac{1}{1 + \left(\frac{\tau + \delta_R - \zeta_1}{w_2 |z_{es}|}\right)^2} \frac{1 - |1/z_{es}|^2}{1 - |1/z_{es}|^{2N}}} \times \left[ \frac{\tau + \delta_R - \zeta_1}{w_2 z_{es}} z_{es}, z_{es}, \dots, \frac{\tau + \delta_R - \zeta_1}{w_2 z_{es}} z_{es}^N, z_{es}^N \right]^T, \quad (23)$$

where

$$0 = w_1 w_2^2 z_{es}^2 + [w_2^3 - w_2(\tau + \delta_R - \zeta_1)^2] z_{es} - w_1(\tau + \delta_R - \zeta_1)^2, \quad (24)$$

$$E = \frac{w_1 w_2 z_{es} + w_2^2}{\tau + \delta_R - \zeta_1} + \zeta_1. \quad (25)$$

But here only the solution with  $|z_{es}| > 1$  is admissible.

Of particular interest is the case  $\tau + \delta_L = \zeta_1$ , where the outermost left site and the bulk sites have the same onsite energies, for which Eqs. (20) and (21) imply that  $z_{es} = -w_1/w_2$  and  $E = \zeta_1$ . If  $w_1/w_2 < 1$  then the eigenstate is localized at the left end with the amplitude given by

$$|\psi_L\rangle^2 = \frac{1 - \left(\frac{w_1}{w_2}\right)^2}{1 - \left(\frac{w_1}{w_2}\right)^{2N}} \begin{bmatrix} 1 \\ 0 \\ \left(\frac{w_1}{w_2}\right)^2 \\ 0 \\ \vdots \\ \left(\frac{w_1}{w_2}\right)^{2(N-1)} \\ 0 \end{bmatrix}. \quad (26)$$

Note that here  $\mathbb{B}_n = 0$  for all  $n$ ; that is, the eigenstate  $|\psi_L\rangle$  is zero on the sublattice of  $S_2$ -type magnetic spheres. For the other case  $\tau + \delta_R = \zeta_1$ , Eqs. (24) and (25) imply that  $z_{es} = -w_2/w_1$  and  $E = \zeta_1$ . If  $w_1/w_2 < 1$  then the eigenstate will be localized at the right end and its amplitude reads

$$|\psi_R\rangle^2 = \frac{1 - \left(\frac{w_1}{w_2}\right)^2}{1 - \left(\frac{w_1}{w_2}\right)^{2N}} \begin{bmatrix} 0 \\ \left(\frac{w_1}{w_2}\right)^{2(N-1)} \\ \vdots \\ 0 \\ \left(\frac{w_1}{w_2}\right)^2 \\ 0 \\ 1 \end{bmatrix}. \quad (27)$$

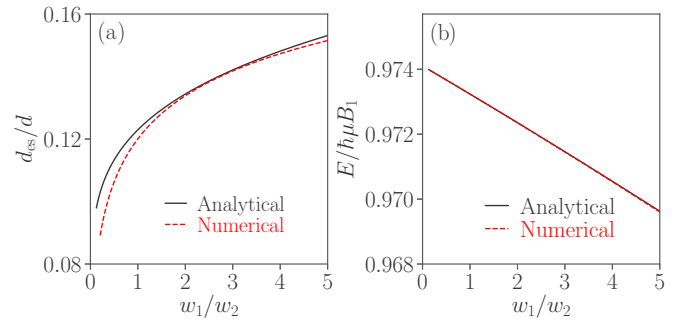


FIG. 3. (a) The localization length  $d_{es}$ , and (b) the energy  $E$  of the left end mode  $|\psi_L\rangle$  versus  $w_1/w_2$ . Analytical and numerical results are denoted by solid and dashed lines, respectively. Here  $N = 80$ ,  $B_1 = B_2 = 0.1$  T,  $d_2 = 6$   $\mu\text{m}$ ,  $S_1 = S_2 = 10^{10}$ ,  $\delta_L = -0.0259E_c$ , and  $\delta_R = 0$ .

But here  $\mathbb{A}_n = 0$  for all  $n$ ; that is, the eigenstate  $|\psi_R\rangle$  is zero on the sublattice of  $S_1$ -type magnetic spheres.

## B. Numerical treatment

Now we go beyond the RWA and consider all  $\hat{\mathbf{a}}_n^\dagger \hat{\mathbf{b}}_n^\dagger$  and similar terms in the Hamiltonian. In the following, we summarize an efficient numerical method to diagonalize quadratic bosonic Hamiltonians given by Colpa [72]. In terms of  $\Phi^\dagger = [\hat{\mathbf{a}}_1^\dagger, \hat{\mathbf{b}}_1^\dagger, \dots, \hat{\mathbf{a}}_N^\dagger, \hat{\mathbf{b}}_N^\dagger]$  the Hamiltonian (3) can be written as

$$H = \frac{1}{2} [\Phi^\dagger \quad \Phi] \tilde{H}_C \begin{bmatrix} \Phi \\ \Phi^\dagger \end{bmatrix}. \quad (28)$$

By using a paraunitary matrix  $\mathcal{T}$ , the matrix  $\tilde{H}_C$  can be put in a diagonal form as

$$\mathcal{T}^\dagger \tilde{H}_C \mathcal{T} = \begin{bmatrix} \mathbf{E} & \mathbf{0} \\ \mathbf{0} & \mathbf{E} \end{bmatrix}. \quad (29)$$

Here  $\mathbf{0}$  is a  $2N \times 2N$  matrix whose elements are zero, and  $\mathbf{E} = \text{diag}[E_1, E_2, \dots, E_{2N}]$ . Introducing  $\chi^\dagger = [\hat{\mathbf{d}}_1^\dagger, \hat{\mathbf{d}}_2^\dagger, \dots, \hat{\mathbf{d}}_{2N}^\dagger]$  via  $[\chi^\dagger \quad \chi] \mathcal{T}^\dagger = [\Phi^\dagger \quad \Phi]$ , the Hamiltonian can be recast into the form

$$H = \frac{1}{2} [\chi^\dagger \quad \chi] \begin{bmatrix} \mathbf{E} & \mathbf{0} \\ \mathbf{0} & \mathbf{E} \end{bmatrix} \begin{bmatrix} \chi \\ \chi^\dagger \end{bmatrix}. \quad (30)$$

The task is now to find the paraunitary matrix  $\mathcal{T}$ . By invoking the Cholesky decomposition, the matrix  $\tilde{H}_C$  can be decomposed as  $\tilde{H}_C = \mathcal{K}^\dagger \mathcal{K}$ , where  $\mathcal{K}$  is an upper triangle matrix. Afterward, a matrix  $\sigma$ , where  $\sigma_{i,j} = \delta_{i,j}$  for  $j = 1, \dots, 2N$  and  $\sigma_{i,j} = -\delta_{i,j}$  for  $j = 2N+1, \dots, 4N$ , is utilized to build the Hermitian matrix  $\mathcal{W} = \mathcal{K} \sigma \mathcal{K}^\dagger$  which can be diagonalized by a unitary matrix  $\mathcal{U}$ , such that  $\mathcal{U}^\dagger \mathcal{W} \mathcal{U} = \tau_z \otimes \mathbf{E}$ . Finally, the paraunitary matrix can be constructed as  $\mathcal{T} = \mathcal{K}^{-1} \mathcal{U} (\tau_0 \otimes \mathbf{E}^{\frac{1}{2}})$ .

Figure 3 shows the localization length  $d_{es}$  and the energy  $E$  of the left end mode as a function of  $w_1/w_2$  obtained from analytical and numerical approaches which are denoted by solid and dashed lines, respectively. The localization length  $d_{es}$  and energy  $E$  of the end states are about the lattice constant  $d$  and the characteristic energy  $E_c \equiv \hbar \mu B_1$ , respectively. The

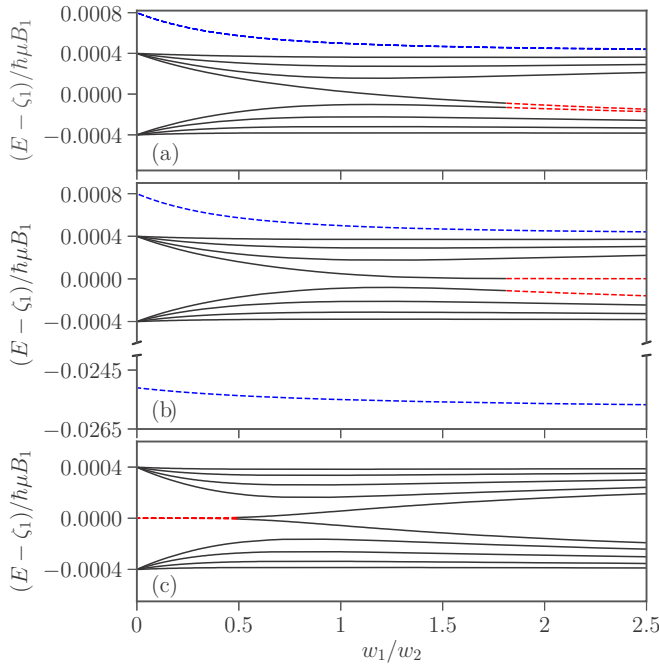


FIG. 4. The energies of a finite chain with  $N = 10$  magnetic spheres versus  $w_1/w_2$ . The energies of bulk states (in black solid) and localized end modes (in dashed) for (a)  $\delta_L = \delta_R = 0$ , (b)  $\delta_L = -0.0259E_c$  and  $\delta_R = 0$ , and (c)  $\delta_L = \delta_R = \zeta_1 - \tau$ . Here  $w_1 + w_2 = -4 \times 10^{-4}E_c$  is kept constant and all the other parameters are the same as in Fig. 3.

analytical results calculated from the RWA approximation are in good agreement with the numerical results derived from the full Hamiltonian, ensuring that the RWA which neglects the quickly oscillating terms is applicable.

We demonstrate how the external onsite energies  $\delta_L$  and  $\delta_R$  and  $w_1/w_2$  affect the nature of the end modes. Moreover, we find the corresponding wave function of the possible end modes, indicating their end localization. Figure 4 shows the energy spectrum as a function of  $w_1/w_2$  for a chain with  $N = 10$ . Here  $w_1 + w_2 = -4 \times 10^{-4}E_c$  and thus  $\zeta_1 = 0.9992E_c$  are kept constant and all the other parameters are the same as in Fig. 3. The energies of the delocalized and localized modes are denoted by solid and dashed lines, respectively. Besides, the wave functions of the various localized end modes for a chain with  $N = 80$  are depicted in Fig. 5.

In the absence of onsite energies  $\delta_L = \delta_R = 0$ , Fig. 4(a), there is a pair of doubly degenerate localized states energetically *above* the delocalized states. Besides, there are two singly degenerate midgap eigenmodes which are delocalized (localized) when  $w_1/w_2$  is smaller (greater) than 1.8 (Note that, in the limit of large  $N$ , the transition point tends to  $w_1/w_2 = 1$ , in all cases). In this case all localized states are Tamm-like states [73]. The corresponding wave functions for the left  $\psi_L$  and right  $\psi_R$  localized states with energies above the gap are shown in Fig. 5(a).

For the case of  $\delta_L \neq 0$  and  $\delta_R = 0$ , Fig. 4(b), there are two singly degenerate localized states, one energetically *above* and one energetically *below* the delocalized states, along with two singly degenerate midgap eigenmodes which are delocalized (localized) when  $w_1/w_2$  is smaller (greater) than 1.8. Despite

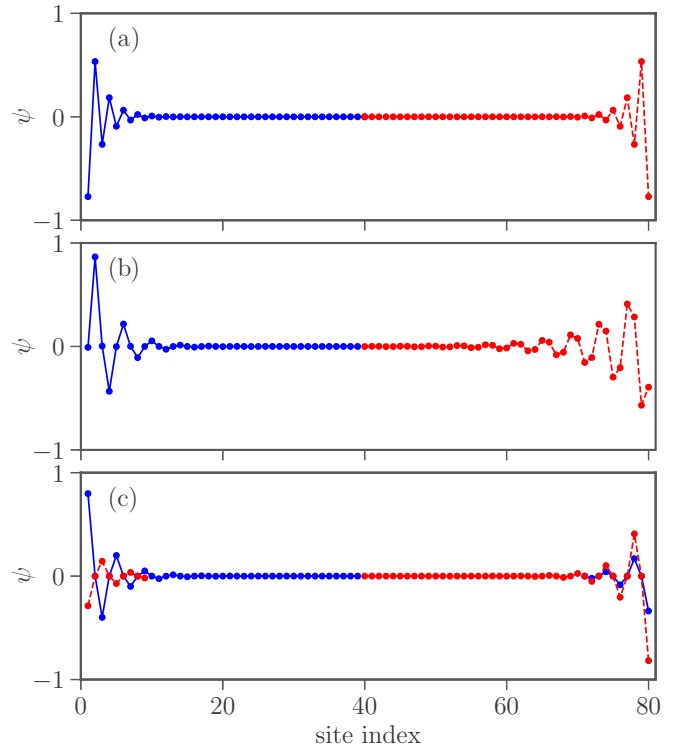


FIG. 5.  $\psi_L$  (in red) and  $\psi_R$  (in blue) for (a)  $\delta_L = \delta_R = 0$  and  $w_1/w_2 = 2$ , (b)  $\delta_L = -0.0259E_c$ ,  $\delta_R = 0$ , and  $w_1/w_2 = 2$ , and (c)  $\delta_L = \delta_R = \zeta_1 - \tau$  and  $w_1/w_2 = 0.5$ . The eigenenergies pertaining to  $(\psi_L, \psi_R)$  are (a)  $(0.9997, 0.9997)E_c$ , (b)  $(0.9992, 0.9991)E_c$ , and (c)  $(0.9992, 0.9992)E_c$ . The wave functions have been calculated for a chain of  $N = 80$  sites. Here  $w_1 + w_2 = -4 \times 10^{-4}E_c$  is kept constant and all the other parameters are the same as in Fig. 3.

having the external onsite energy at one of the chain ends, all localized states are Tamm-like states. The corresponding wave functions for the localized states with energies within the gap are plotted in Fig. 5(b).

The case of  $\delta_L = \delta_R = \zeta_1 - \tau$ , where onsite energies of the outermost and the bulk sites are equal, is of particular interest. Figure 4(c) shows that here all states are singly degenerate delocalized states when  $w_1/w_2 > 0.5$  while for  $w_1/w_2 < 0.5$ , a pair of *doubly degenerate* localized modes appear within the gap, which are topological end states. For  $w_1/w_2 < 1$  the system is in a topological phase characterized by  $\varphi_{\text{Zak}} = \pi$  and is thus expected to host localized topologically protected edge states imposed by the bulk-boundary correspondence. The wave functions for the localized end states in this case are depicted in Fig. 5(c). Therefore, the type of end modes is determined by the additional magnetic inductions applied at the end sites of the chain.

To examine the robustness of the edge states against perturbations, we add  $H_{\text{perturb}} = w_{\text{perturb}} \sum_{n=1}^{N-1} (\hat{\mathbf{a}}_n \hat{\mathbf{a}}_{n+1} + \hat{\mathbf{b}}_n \hat{\mathbf{b}}_{n+1} + \text{H.c.})$  to the Hamiltonian (3). In other words, we add

$$\mathcal{H}_{\text{perturb}}(k) = w_{\text{perturb}} \begin{bmatrix} 0 & e^{-ikd} \\ e^{ikd} & 0 \end{bmatrix} \otimes \tau_0$$

to the Hamiltonian (4). We find that, despite the presence of this perturbation, the Zak phase of an infinite chain with

$\zeta_1 = \zeta_2$  persists to be quantized, and topological end states of a finite chain persist to be present. Indeed, topological end states are protected against perturbations that preserve the inversion symmetry  $\mathcal{I}\mathcal{H}_{\text{perturb}}(k)\mathcal{I}^{-1} = \mathcal{H}_{\text{perturb}}(-k)$  where  $\mathcal{I} = \tau_x \otimes \tau_x$ .

### V. EDGE STATES AT THE INTERFACE OF TWO TOPOLOGICALLY DISTINCT CHAINS

Now we study the existence of topologically protected edge states at the interface between two topologically distinct subchains of magnetic spheres, characterized by different Zak phases  $\varphi_{\text{zak}} = 0$  and  $\varphi_{\text{zak}} = \pi$ . We assume that the left and right subchains consist of  $N$  and  $N + 1$  magnetic spheres, respectively, where  $N$  is an even integer. The unit cell of the left and the right subchains is identified with a pair of distances  $(d_1, d_2)$  and  $(d'_1, d'_2)$ , respectively, such that  $d = d_1 + d_2$  and  $d' = d'_1 + d'_2$ . Without loss of generality, we choose  $d'_2 = d_2$ . The energy  $w_J$  characterizes the junction of the two subchains.

The bulk sites of the left (right) subchain have the onsite energy  $\zeta_1$  ( $\zeta'_1$ ), while the end sites of the left (right) subchain have the onsite energies  $\tau + \delta_L$  and  $\tau + \delta_R$  ( $\tau'_L + \delta'_L$  and  $\tau'_R + \delta'_R$ ), where

$$\begin{aligned}\tau &= -\frac{\mu_0 \hbar^2 \mu^2}{4\pi d_1^3} S_1 + \hbar \mu B_1, \\ \tau'_L &= -\frac{\mu_0 \hbar^2 \mu^2}{4\pi d_1^3} S_1 + \hbar \mu B_1, \\ \tau'_R &= -\frac{\mu_0 \hbar^2 \mu^2}{4\pi d_2^3} S_1 + \hbar \mu B_1.\end{aligned}\quad (31)$$

We analytically verify the formation of the localized edge state at the interface. To this end, we rely on the RWA and assume that the bulk and the end sites of each left and right subchains have the same onsite energies and solve for the eigenmode  $|\psi\rangle = [\mathbb{A}_1, \mathbb{B}_1, \dots, \mathbb{A}_N, \mathbb{B}_N, \mathbb{A}_{N+1}, \mathbb{B}_{N+1}, \dots, \mathbb{A}_{2N+1}]^T$  of  $\mathfrak{h}$  given in the appendix. By considering the ansatz

$$\begin{aligned}\mathbb{A}_l &= \frac{\mathbb{A}_N}{z_{\text{es}}^{N-l}} \text{ for } 1 \leq l \leq N, \\ \mathbb{B}_l &= \frac{\mathbb{B}_N}{z_{\text{es}}^{N-l}} \text{ for } 1 \leq l \leq N, \\ \mathbb{A}_l &= \mathbb{A}_{N+1} z'_{\text{es}}{}^{l-N-1} \text{ for } N+1 \leq l \leq 2N+1, \\ \mathbb{B}_l &= \mathbb{B}_{N+1} z'_{\text{es}}{}^{l-N-1} \text{ for } N+1 \leq l \leq 2N.\end{aligned}\quad (32)$$

and following the procedure outlined in Sec. IV A, we end up with

$$\begin{aligned}0 &= \sqrt{\left(\frac{w_1}{w_2}\right)^2 + \frac{w_1}{w_2} \left(z_{\text{es}} + \frac{1}{z_{\text{es}}}\right)} + 1 - \frac{(\zeta_1 - \zeta'_1)}{w_2} \\ &\quad + \sqrt{\left(\frac{w'_1}{w_2}\right)^2 + \frac{w'_1}{w_2} \left(z'_{\text{es}} + \frac{1}{z'_{\text{es}}}\right)} + 1, \\ 0 &= \sqrt{\frac{w_2/z_{\text{es}} + w_1}{w_2 z_{\text{es}} + w_1}} \sqrt{\frac{w_2 z'_{\text{es}} + w'_1}{w_2/z'_{\text{es}} + w'_1}} + \frac{z'_{\text{es}}}{z_{\text{es}}} \left(\frac{w_J}{w_2}\right)^2.\end{aligned}\quad (33)$$

Note that here only eigenstates with  $|z_{\text{es}}| > 1$  and  $|z'_{\text{es}}| < 1$  are admissible. Indeed, the localization lengths  $d_{\text{es}} = d/|\ln |z_{\text{es}}||$  and  $d'_{\text{es}} = d'/|\ln |z'_{\text{es}}||$  characterize the decay of the edge state inside the left and right subchains, respectively. Moreover, it turns out that

$$\begin{aligned}\mathbb{A}_{N+1} &= \mathbb{A}_N \frac{w_2}{w_J} z_{\text{es}}, \\ \mathbb{B}_N &= -\mathbb{A}_N \sqrt{\frac{w_2 z_{\text{es}} + w_1}{w_2/z_{\text{es}} + w_1}}, \\ \mathbb{B}_{N+1} &= -\mathbb{A}_N \frac{w_J}{w_2} z'_{\text{es}} \sqrt{\frac{w_2 z_{\text{es}} + w_1}{w_2/z_{\text{es}} + w_1}},\end{aligned}\quad (34)$$

where

$$\begin{aligned}|\mathbb{A}_N|^2 &= \left[ \frac{1 - 1/z_{\text{es}}^{2N}}{1 - 1/z_{\text{es}}^2} \frac{w_2(z_{\text{es}} + 1/z_{\text{es}}) + 2w_1}{w_2/z_{\text{es}} + w_1} \right. \\ &\quad + \left| \frac{w_2 z_{\text{es}}}{w_J} \right|^2 \frac{1 - z'_{\text{es}}{}^{2N+2}}{1 - z'_{\text{es}}{}^2} \\ &\quad \left. + \left| \frac{w_J z'_{\text{es}}}{w_2} \right|^2 \frac{w_2 z_{\text{es}} + w_1}{w_2/z_{\text{es}} + w_1} \frac{1 - z'_{\text{es}}{}^{2N}}{1 - z'_{\text{es}}{}^2} \right]^{-1}.\end{aligned}\quad (35)$$

Now using Eq. (32), the eigenstate  $|\psi\rangle$  can be determined straightforwardly.

The appearance of the localized edge state is also verified numerically by going beyond the RWA. We consider a chain composed of two subchains with 60 and 61 magnetic spheres. Figures 6(a)–6(c) show the localization length for each subchain  $d_{\text{es}}$ ,  $d'_{\text{es}}$  and the energy spectrum  $E$  for various  $w_1$  and  $w'_1$ . Even though the analytical results are calculated within the RWA, they are in good agreement with the full numerical results. Figure 6(d) demonstrates that, at the domain wall formed between two subchains, an edge state forms at the midgap energy. It is worth noting that, when both subchains are sharing the same topological invariant, there is no edge state at the interface. The localized edge state in Fig. 6(d) exponentially decays away from the interface with different decay lengths,  $d_{\text{es}}$  and  $d'_{\text{es}}$ . Due to the broken mirror symmetry around the interface, the localized edge state is neither anti-symmetric nor symmetric.

### VI. DISCUSSION

The gap between the two excitation branches for the translationally invariant chain of magnetic spheres can be closed if  $w_1 = w_2$  and  $\zeta_1 = \zeta_2$ , which leads to  $E_{1k} = E_{2k} = \zeta_1$ . The characteristic energy of the localized eigenmode at the left and right ends of a finite chain is  $\zeta_1$  when  $z_{\text{es}} = -w_1/w_2$  and  $z_{\text{es}} = -w_2/w_1$ , respectively, which is possible only if the onsite energies of end sites are equal to  $\zeta_1$ . The nature of the localized states is determined by the onsite energies of the chain bulk and end sites. Tamm-like states can form with an energy higher or lower than  $\zeta_1$ , while topological end states with energy  $\zeta_1$  occurs only if  $w_1/w_2 < 1$  and  $\tau + \delta_L = \zeta_1$  or  $\tau + \delta_R = \zeta_1$ . Moreover, the topological end states are protected against perturbations that do not break the inversion symmetry. Thus the *existence* and nature of localized end

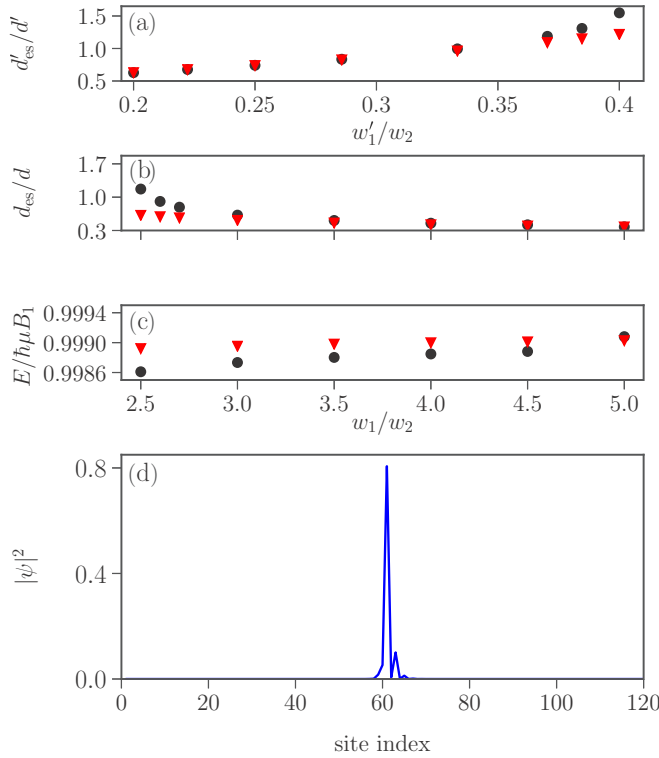


FIG. 6. The analytical (circle) and numerical (triangle) results for (a)  $d'_{es}$  as a function of  $w'_1/w_2$ , (b)  $d_{es}$ , and (c)  $E$  as a function of  $w_1/w_2$ . (d)  $|\psi|^2$  of the localized state at the interface of two subchains for  $w_1/w_2 = 3$ ,  $\zeta_1 = 0.9966E_c$ , and  $\zeta'_1 = 0.9989E_c$ . In all panels  $(w_1/w_2)(w'_1/w_2) = 1$ ,  $w_1 = w_2$ ,  $N = 60$  and the other parameters are the same as in Fig. 3.

states of a chain of magnetic spheres can be controlled by the external magnetic fields.

The analytical and numerical results for the localization length  $d_{es}$  and energy  $E$  of localized states are in good agreement (Fig. 3). This confirms that the RWA is applicable when the frequency  $(\zeta_1 + \zeta_2)/\hbar$  is much larger than the hopping frequencies  $|w_1|/\hbar$  and  $|w_2|/\hbar$ . Whether the RWA breaks down has no influence on the topology of the system, but on the *symmetry* of its energy spectrum; see Fig. 7.

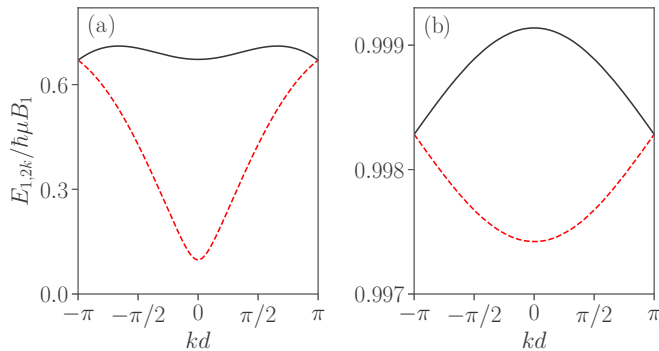


FIG. 7. The bulk excitation spectrum  $E_{1k}$  (in black solid) and  $E_{2k}$  (in red dashed) as a function of  $kd$  for (a)  $B_1 = B_2 = 0.55$  mT, and (b)  $B_1 = B_2 = 100$  mT. Here  $d_1 = d_2 = 6 \mu\text{m}$  and  $S_1 = S_2 = 10^{10}$ .

Remarkably, comparatively low magnetic inductions  $\delta B_{L,R} \sim 1$  mT are required to control the system. Despite the micrometer separation of spheres, no practical difficulties arise in applying the external fields: Only the outermost left and right spheres with a separation of  $\sim 1$  mm should experience extra *local* magnetic inductions while all spheres are subjected to a weak *uniform* field  $B_{1,2} \sim 100$  mT.

Our analysis suggests a physical realization of a magnonic waveguide in which the guided modes are due to the dipolar coupling among magnetic spheres with small magnetic loss and high values of saturation magnetization, and give rise to the transmission of spin waves with highly suppressed backscattering. This opens up novel opportunities to explore the capability of an information-carrying spin wave for future use in technologies. Moreover, magnetic spheres in cavities have been demonstrated to hybridize with optical [74,75] and microwave photons [69,70]. Our study paves the way towards utilizing a chain of magnetic spheres for bidirectional conversion between optical and microwave photons, which is of prime importance in the realm of long-distance quantum communication.

## VII. CONCLUSION

In conclusion, we have introduced a magnonic crystal, a linear bipartite chain of dipolarly coupled magnetic spheres, which to some extent provides a spin wave analogy with the SSH model which is able to host topologically protected end states. We specified the fundamental properties of collective excitations in the magnetic chain with a two-site unit cell. We obtained the Zak phase associated with the magnonic bands to classify topologically distinct phases. We also investigated various types of localized end states that may exist in a finite chain both analytically and numerically. Our results indicate that not only Tamm-like localized states but also topological end states may form at the boundaries of the system. The nature of end modes that may form is determined by the onsite energies of the bulk and end sites. The external magnetic fields thus can be used to control the Tamm-like localized states, topological end states, energy spectrum, energy gap, and other properties of the chain.

The electric and magnetic dipolar interactions are quite similar, hence topological chains of metallic nanoparticles [76] and magnetic microspheres may share some common features. However, a bipartite chain composed of magnetic *microspheres* is easier to realize experimentally. The *micrometer* separation of spheres can also be changed to tune the topological chain. Notably the external magnetic fields can be utilized to dramatically change the characteristics of the magnetic chain. Therefore, a chain of magnetic spheres provides a promising *dynamically reconfigurable* system.

## APPENDIX

Relying on the RWA, the approximate Hamiltonian in the basis  $\Phi^\dagger = [\hat{\mathbf{a}}_1^\dagger, \hat{\mathbf{b}}_1^\dagger, \dots, \hat{\mathbf{a}}_{2N+1}^\dagger]$  can be expressed as



$H = \Phi^\dagger \mathfrak{h} \Phi$ , where  $\mathfrak{h}$  is given by

$$\mathfrak{h} = \begin{bmatrix} \tau + \delta_L & w_1 & 0 & 0 & \cdots & 0 & 0 & 0 & 0 & 0 & 0 & 0 & \cdots & 0 & 0 & 0 \\ w_1 & \zeta_1 & w_2 & 0 & \cdots & 0 & 0 & 0 & 0 & 0 & 0 & 0 & \cdots & 0 & 0 & 0 \\ 0 & w_2 & \zeta_1 & w_1 & \cdots & 0 & 0 & 0 & 0 & 0 & 0 & 0 & \cdots & 0 & 0 & 0 \\ \vdots & \vdots & \ddots & \ddots & \ddots & \vdots & \vdots & \vdots & \vdots & \vdots & \vdots & \vdots & \cdots & \vdots & \vdots & \vdots \\ 0 & 0 & 0 & 0 & \cdots & w_2 & \zeta_1 & w_1 & 0 & 0 & 0 & 0 & \cdots & 0 & 0 & 0 \\ 0 & 0 & 0 & 0 & \cdots & 0 & w_1 & \tau + \delta_R & w_1 & 0 & 0 & 0 & \cdots & 0 & 0 & 0 \\ 0 & 0 & 0 & 0 & \cdots & 0 & 0 & w_1 & \tau'_L + \delta'_L & w'_1 & 0 & 0 & \cdots & 0 & 0 & 0 \\ 0 & 0 & 0 & 0 & \cdots & 0 & 0 & 0 & w'_1 & \zeta'_1 & w_2 & 0 & \cdots & 0 & 0 & 0 \\ 0 & 0 & 0 & 0 & \cdots & 0 & 0 & 0 & 0 & w_2 & \zeta'_1 & w'_1 & \cdots & 0 & 0 & 0 \\ \vdots & \vdots & \vdots & \vdots & \vdots & \vdots & \vdots & \vdots & \vdots & \vdots & \ddots & \ddots & \ddots & \vdots & \vdots & \vdots \\ 0 & 0 & 0 & 0 & 0 & 0 & 0 & 0 & 0 & 0 & 0 & 0 & \cdots & w'_1 & \zeta'_1 & w_2 \\ 0 & 0 & 0 & 0 & 0 & 0 & 0 & 0 & 0 & 0 & 0 & 0 & \cdots & 0 & w_2 & \tau'_R + \delta'_R \end{bmatrix}. \quad (\text{A1})$$

- [1] B. Lenk, H. Ulrichs, F. Garbs, and M. Münzenberg, *Phys. Rep.* **507**, 107136 (2011).
- [2] A. A. Serga, A. V. Chumak, and B. Hillebrands, *J. Phys. D: Appl. Phys.* **43**, 264002 (2010).
- [3] V. V. Kruglyak and R. J. Hicken, *J. Magn. Magn. Mater.* **306**, 191 (2006).
- [4] V. V. Kruglyak, S. O. Demokritov, and D. Grundler, *J. Phys. D: Appl. Phys.* **43**, 264001 (2010).
- [5] A. V. Chumak, V. I. Vasyuchka, A. A. Serga, and B. Hillebrands, *Nat. Phys.* **11**, 453 (2015).
- [6] M. Krawczyk and D. Grundler, *J. Phys.: Condens. Matter* **26**, 123202 (2014).
- [7] A. V. Chumak, T. Neumann, A. A. Serga, B. Hillebrands, and M. P. Kostylev, *J. Phys. D: Appl. Phys.* **42**, 205005 (2009).
- [8] A. Khitun, M. Bao, and K. L. Wang, *J. Phys. D: Appl. Phys.* **43**, 264005 (2010).
- [9] Z. K. Wang, V. L. Zhang, H. S. Lim, S. C. Ng, M. H. Kuok, S. Jain, and A. O. Adeyeye, *Appl. Phys. Lett.* **94**, 083112 (2009).
- [10] M. Krawczyk, S. Mamica, J. W. Klos, J. Romero-Vivas, M. Mruczkiewicz, and A. Barman, *J. Appl. Phys.* **109**, 113903 (2011).
- [11] G. Gubbiotti, S. Tacchi, M. Madami, G. Carlotti, A. O. Adeyeye, and M. Kostylev, *J. Phys. D: Appl. Phys.* **43**, 264003 (2010).
- [12] F. S. Ma, H. S. Lim, Z. K. Wang, S. N. Piramanayagam, S. C. Ng, and M. H. Kuok, *Appl. Phys. Lett.* **98**, 153107 (2011).
- [13] C. H. O. Costa, M. S. Vasconcelos, and E. L. Albuquerque, *J. Appl. Phys.* **109**, 07D319 (2011).
- [14] G. Gubbiotti, G. Carlotti, P. Vavassori, M. Kostylev, N. Singh, S. Goolaup, and A. O. Adeyeye, *Phys. Rev. B* **72**, 224413 (2005).
- [15] Z. K. Wang, V. L. Zhang, H. S. Lim, S. C. Ng, M. H. Kuok, S. Jain, and A. O. Adeyeye, *ACS Nano* **4**, 643 (2010).
- [16] J. Topp, D. Heitmann, M. P. Kostylev, and D. Grundler, *Phys. Rev. Lett.* **104**, 207205 (2010).
- [17] N. I. Polushkin, *Phys. Rev. B* **82**, 172405 (2010).
- [18] G. Gubbiotti, S. Tacchi, G. Carlotti, N. Singh, S. Goolaup, A. O. Adeyeye, and M. Kostylev, *Appl. Phys. Lett.* **90**, 092503 (2007).
- [19] M. Krawczyk, J. Klos, M. L. Sokolovskyy, and S. Mamica, *J. Appl. Phys.* **108**, 093909 (2010).
- [20] S. A. Nikitov, Ph. Tailhades, and C. S. Tsai, *J. Magn. Magn. Mater.* **236**, 320 (2001).
- [21] S.-K. Kim, *J. Phys. D: Appl. Phys.* **43**, 264004 (2010).
- [22] E. Yablonovitch, *Phys. Rev. Lett.* **58**, 2059 (1987).
- [23] S. John, *Phys. Rev. Lett.* **58**, 2486 (1987).
- [24] M.-H. Lu, L. Feng, and Y.-F. Chen, *Mater. Today (Oxford, U. K.)* **12**, 34 (2009).
- [25] Z. Liu, X. Zhang, Y. Mao, Y. Y. Zhu, Z. Yang, C. T. Chan, and P. Sheng, *Science* **289**, 1734 (2000).
- [26] J. O. Vasseur, L. Dobrzynski, B. Djafari-Rouhani, and H. Puszkarski, *Phys. Rev. B* **54**, 1043 (1996).
- [27] B. Zare Rameshti, Y. Cao, and G. E. W. Bauer, *Phys. Rev. B* **91**, 214430 (2015).
- [28] B. Zare Rameshti, and G. E. W. Bauer, *Phys. Rev. B* **97**, 014419 (2018).
- [29] Y. Zhu, K. H. Chi, and C. S. Tsai, *Appl. Phys. Lett.* **105**, 022411 (2014).
- [30] H. Takagi, J. Noda, T. Ueno, N. Kanazawa, Y. Nakamura, and M. Inoue, *Electron. Commun. Jpn.* **97**, 833 (2014).
- [31] A. V. Chumak, A. A. Serga, and B. Hillebrands, *Nat. Commun.* **5**, 4700 (2014).
- [32] L. Lu, J. D. Joannopoulos, and M. Soljačić, *Nat. Photonics* **8**, 821 (2014).
- [33] A. B. Khanikaev and G. Shvets, *Nat. Photonics* **11**, 763 (2017).
- [34] T. Ozawa, H. M. Price, A. Amo, N. Goldman, M. Hafezi, L. Lu, M. Rechtsman, D. Schuster, J. Simon, O. Zilberberg, and I. Carusotto, *arXiv:1802.04173*.
- [35] C. He, X. Ni, H. Ge, X.-C. Sun, Y.-B. Chen, M.-H. Lu, X.-P. Liu, and Y.-F. Chen, *Nat. Phys.* **12**, 1124 (2016).
- [36] R. Fleury, A. B. Khanikaev, and A. Alù, *Nat. Commun.* **7**, 11744 (2016).

- [37] Z. Yang, F. Gao, X. Shi, X. Lin, Z. Gao, Y. Chong, and B. Zhang, *Phys. Rev. Lett.* **114**, 114301 (2015).
- [38] V. Peano, C. Brendel, M. Schmidt, and F. Marquardt, *Phys. Rev. X* **5**, 031011 (2015).
- [39] F. D. M. Haldane and S. Raghu, *Phys. Rev. Lett.* **100**, 013904 (2008).
- [40] S. Raghu and F. D. M. Haldane, *Phys. Rev. A* **78**, 033834 (2008).
- [41] C. Zhang and Q. Niu, *Phys. Rev. A* **81**, 053803 (2010).
- [42] Z. Wang, Y. Chong, J. D. Joannopoulos, and M. Soljčić, *Nature (London)* **461**, 772 (2009).
- [43] P. Wang, L. Lu, and K. Bertoldi, *Phys. Rev. Lett.* **115**, 104302 (2015).
- [44] T. Ma, A. B. Khanikaev, S. H. Mousavi, and G. Shvets, *Phys. Rev. Lett.* **114**, 127401 (2015).
- [45] L.-H. Wu and X. Hu, *Phys. Rev. Lett.* **114**, 223901 (2015).
- [46] T. Ma and G. Shvets, *New J. Phys.* **18**, 025012 (2016).
- [47] S. Barik, H. Miyake, W. DeGottardi, E. Waks, and M. Hafezi, *New J. Phys.* **18**, 113013 (2016).
- [48] S. H. Mousavi, A. B. Khanikaev, and Z. Wang, *Nat. Commun.* **6**, 8682 (2015).
- [49] T.-W. Liu and F. Semperlotti, *Phys. Rev. Appl.* **9**, 014001 (2018).
- [50] A. Kanshu, C. E. Rüter, D. Kip, V. Shandarov, P. P. Beličev, I. Ilić, and M. Stepić, *Opt. Lett.* **37**, 1253 (2012).
- [51] H. Schomerus, *Opt. Lett.* **38**, 1912 (2013).
- [52] C. Poli, M. Bellec, U. Kuhl, F. Mortessagne, and H. Schomerus, *Nat. Commun.* **6**, 6710 (2015).
- [53] A. P. Slobozhanyuk, A. N. Poddubny, A. E. Miroshnichenko, P. A. Belov, and Y. S. Kivshar, *Phys. Rev. Lett.* **114**, 123901 (2015).
- [54] L. Zhang, J. Ren, J. S. Wang, and B. Li, *Phys. Rev. B* **87**, 144101 (2013).
- [55] A. Mook, J. Henk, and I. Mertig, *Phys. Rev. B* **90**, 024412 (2014).
- [56] R. Chisnell, J. S. Helton, D. E. Freedman, D. K. Singh, R. I. Bewley, D. G. Nocera, and Y. S. Lee, *Phys. Rev. Lett.* **115**, 147201 (2015).
- [57] S. A. Owerre, *Sci. Rep.* **7**, 6931 (2017).
- [58] W. P. Su, J. R. Schrieffer, and A. J. Heeger, *Phys. Rev. Lett.* **42**, 1698 (1979).
- [59] J. Ruostekoski, G. V. Dunne, and J. Javanainen, *Phys. Rev. Lett.* **88**, 180401 (2002).
- [60] A. J. Heeger, S. Kiverson, J. R. Schrieffer, and W. P. Su, *Rev. Mod. Phys.* **60**, 781 (1988).
- [61] R. Jackiw and C. Rebbi, *Phys. Rev. D* **13**, 3398 (1976).
- [62] E. J. Meier, F. Alex An, and B. Gadway, *Nat. Commun.* **7**, 13986 (2016).
- [63] M. Xiao, G. Ma, Z. Yang, P. Sheng, Z. Q. Zhang, and C. T. Chan, *Nat. Phys.* **11**, 240 (2015).
- [64] M. Atala, M. Aidelsburger, J. T. Barreiro, D. Abanin, T. Kitagawa, E. Demler, and I. Bloch, *Nat. Phys.* **9**, 795 (2013).
- [65] J. M. Zeuner, M. C. Rechtsman, Y. Plotnik, Y. Lumer, S. Nolte, M. S. Rudner, M. Segev, and A. Szameit, *Phys. Rev. Lett.* **115**, 040402 (2015).
- [66] W. Tan, Y. Sun, H. Chen, and S.-Q. Shen, *Sci. Rep.* **4**, 3842 (2014).
- [67] Ö. O. Soykal and M. E. Flatté, *Phys. Rev. Lett.* **104**, 077202 (2010).
- [68] H. Huebl, C. W. Zollitsch, J. Lotze, F. Hocke, M. Greifenstein, A. Marx, R. Gross, and S. T. B. Goennenwein, *Phys. Rev. Lett.* **111**, 127003 (2013).
- [69] Y. Tabuchi, S. Ishino, T. Ishikawa, R. Yamazaki, K. Usami, and Y. Nakamura, *Phys. Rev. Lett.* **113**, 083603 (2014).
- [70] X. Zhang, C.-L. Zou, L. Jiang, and H. X. Tang, *Phys. Rev. Lett.* **113**, 156401 (2014).
- [71] J. Zak, *Phys. Rev. Lett.* **62**, 2747 (1989).
- [72] J. H. P. Colpa, *Phys. A (Amsterdam, Neth.)* **93**, 327 (1978).
- [73] I. E. Tamm, *Eur. Phys. J. A* **76**, 849 (1932).
- [74] J. A. Haigh, S. Langenfeld, N. J. Lambert, J. J. Baumberg, A. J. Ramsay, A. Nunnenkamp, and A. J. Ferguson, *Phys. Rev. A* **92**, 063845 (2015).
- [75] R. Hisatomi, A. Osada, Y. Tabuchi, T. Ishikawa, A. Noguchi, R. Yamazaki, K. Usami, and Y. Nakamura, *Phys. Rev. B* **93**, 174427 (2016).
- [76] C. A. Downing and G. Weick, *Phys. Rev. B* **95**, 125426 (2017).